Experimental Thermal and Fluid Science 34 (2010) 1353–1366

Contents lists available at ScienceDirect

Experimental Thermal and Fluid Science

journal homepage: www.elsevier.com/locate/etfs

Characterization of high-pressure water-mist sprays: Experimental analysis of droplet size and dispersion

Paolo E. Santangelo *,[1]

Dipartimento di Ingegneria Meccanica e Civile, Università degli Studi di Modena e Reggio Emilia, Via Vignolese 905/b, 41125 Modena, Italy

ARTICLE INFO

Article history:
Received 22 March 2010
Received in revised form 16 June 2010
Accepted 16 June 2010

Keywords:
Water mist
Spray characterization
Atomization degree
Dispersion
Laser-based techniques

ABSTRACT

Popularity of water mist is increasing for a variety of applications within the broad areas of fire suppression and surface cooling. The present study has been focused on characterizing the solid-cone water-mist spray produced by a typical atomizer at high operative pressure (in the range 60–80 bar). To this end, an experimental campaign has been conducted, mainly employing optical techniques: drop-size and flux distribution, initial velocity and cone angle have been investigated to provide a quantitative description of atomization and dispersion.

Most notably, a laser-diffraction-based instrument (*Malvern Spraytec*) has been used to evaluate drop size, while velocity field and spray-cone angle have been studied by Particle Image Velocimetry (PIV) technique. Appropriate measurement methodologies have been developed to the purpose. Moreover, a theoretical discussion based on inviscid-fluid assumption is presented and some relations have been evaluated as predictive of the considered parameters.

1. Introduction

Water-mist systems have recently become a promising technology for a variety of applications within the fields of fire protection and surface cooling. With regard to the former, their market appeal has started since hydrogenated hydrocarbons (commonly known as *halons*) were *de facto* banned in 1987, because of their impact on the ozone layer. Water-mist fire-suppression systems are currently employed for both stationary (residential and industrial) and mobile (aeronautic and naval) applications. Most notably, shipboard applications represented the first test case for researchers and designers: a remarkable share of the open literature in the field consists of the studies realized by the US Navy [1–3]. Other fundamental analyses have been carried out by Lentati and Chelliah [4], Thomas [5] and Chelliah [6] to investigate the physical phenomena occurring in fire suppression by water mist. However, the mentioned works are either mainly or totally focused on suppression mechanisms and flow-flame interaction: most studies in the field have been aimed at analyzing suppression performance, but only limited researches have been conducted to investigate the spray characteristics of these systems. The present work has been realized to the purpose, standing in the frame of a wider research on experimental characterization and numerical simulation of water-mist sprays [7–9]. It is noteworthy to mention the early study by Wang et al. [10] and the recent work by Paulsen Husted et al. [11], that strongly inspired the present research with specific regard to the experimental approach and the investigated parameters.

Transport phenomena in water-mist sprays are connected to operative pressure (usually greater than 35 bar [12]) and relatively small drops (characteristic diameter D_{v99} lower than 1000 μm at 1 m distance from the nozzle [12]). These two features emphasize the capability of spreading water droplets over a large area and cooling the surrounding fluid through the evaporation process, while potential difficulties arise in interacting with fire and overtaking potential obstructions. Transport and suppression depend on atomization and dispersion: the present work is aimed at providing a quantitative evaluation of these two major aspects through the experimental measurement of some parameters. Most notably, drop-size distribution and characteristic diameter of the spray yield to a clear representation of the atomization degree [13], while velocity field and spray-cone angle are representative of dispersion, even if this latter is also connected to drop size as well [13]. Water mist is commonly generated by pressure-swirl atomizers; a large body of literature is available on the characterization of sprays produced by this nozzle typology, with particular reference to the propulsion field. Among the fundamental works, Yule and Widger [14] investigated high-pressure water sprays, while Senecal et al. [15] carried out a research on the linear stability of high-speed viscous liquid sheet, with strong relation to fuel jets.

* Tel.: +39 059 205 6313; fax: +39 059 205 6126.
E-mail address: paoloemilio.santangelo@unimore.it
[1] Former Affiliation: Department of Fire Protection Engineering, University of Maryland, 3106 J.M. Patterson Building, College Park, MD 20742, USA.

0894-1777/$ - see front matter © 2010 Elsevier Inc. All rights reserved.
doi:10.1016/j.expthermflusci.2010.06.008

Nomenclature

A	generic point at the cone boundary (Fig. 12)
CVF	Cumulative Volume Fraction
D	droplet diameter (μm)
D_i	diameter of the injector outlet (mm)
D_{v50}	characteristic diameter, having 50% of the sprayed droplets a smaller diameter (μm)
Disp	data percentage dispersion
FN	flow number (l min^{-1} bar$^{-0.5}$)
$\dot{m}$	mass-flow rate (kg s^{-1})
M	total number of measured drop sizes
MV	mean value
n	number of droplets
N	total number of drop-size-measurement locations
p	static pressure (Pa, bar)
P	total pressure (Pa, bar)
q''	mass flux (kg m^{-2} s^{-1})
Q	volumetric flow rate (m^3 s^{-1})
r	radial coordinate (m)
R	radius (m)
SD	standard deviation
SMD, D_{32}	Sauter Mean Diameter (μm, m)
V	velocity magnitude (m s^{-1})
V''	volumetric flux (m s^{-1})
VF	volume fraction
x	spatial coordinate
y	spatial coordinate
Z	generic number of tests

Greek symbols

γ	curve-fitting coefficient in the Rosin–Rammler log-normal distribution
γ'	parameter defined by Eq. (6)
ν	kinematic viscosity (m^2 s^{-1})
θ	half cone angle (°, rad)
ρ	density (kg m^{-3})
σ	surface tension (N m^{-1})
ξ	generic parameter

Subscripts

1	inlet section of the injector
2	outlet section of the injector
atm	atmospheric
CVF	Cumulative Volume Fraction
Drop Size	drop-size measurements
extr	extrapolated
j	index to the *j*th quantity
k	index to the *k*th quantity
meas	measured
PG	pressure gauge
reconstr	reconstructed
total	total

With regard to experimental studies, drop size of sprays has represented a challenge for decades as a parameter to be quantitatively determined. A prominent reference is the work by Azzopardi [16], where a basic understanding of the possible methodologies and techniques is provided. As expected, remarkable results have been achieved with relation to internal combustion engines, being the size of injected fuel droplets a key parameter in that field [17–19]. In the present work, drop-size measurements have been carried out employing the *Malvern Spraytec*, a laser-based instrument developed by Swithenbank et al. [20]: laser diagnostics has become very common for many applications in multiphase fluid dynamics, as shown and surveyed by Bachalo [21] and Rinkevichius [22]. The *Malvern Spraytec* has also been employed by Chaker et al. [23] to measure drop-size distribution in gas-turbine fogging: their study refers to an application of water-mist sprays different from fire suppression. Interest in water-mist cooling of gas-turbine blades has been shown for decades [24,25], as well as the more general mist cooling of heated surfaces [26,27]. However, these studies are strongly focused on the heat-transfer mechanisms, rather than the transport phenomena of the spray. The recent work by Ren et al. [28] constitutes one of the few references on *Malvern Spraytec* applications in the fire-protection field, with specific regard to drop-size measurements of traditional-sprinkler sprays.

Initial velocity of the water-mist spray has been investigated employing Particle Image Velocimetry (PIV). This technique has been developed three decades ago [29] and has gained wide popularity in fluid-dynamics researches. However, few works have been conducted in fire-suppression field through PIV: Sheppard and Lueptow [30] focused on traditional-sprinkler sprays, while Presser et al. [31] studied water-mist flow over different kinds of obstacle. The already mentioned study by Wang et al. [10] stands as a prominent reference for the present work, even if conducted at low pressure (2–8 bar): PIV images are employed to determine both drop size and mean velocity, together with some evaluation of cone angle and breakup length. The present research may thus serve as an advancement towards higher values of operative pressure. The already mentioned recent work by Paulsen Husted et al. [11] focuses on comparing PIV with PDA (Phase Doppler Anemometry) measurements in water-mist sprays. On the other hand, a large body of references is available on PIV applied to analyze Gasoline Direct Injection (GDI) systems [32,33]. It is also worthwhile to mention the work by Boëdec and Simoëns [34] on velocity fields of the two phases (droplets and gas) in high-pressure sprays.

In the present work, an experimental characterization of the spray produced by a water-mist injector is proposed in terms of both atomization degree (droplet size at 1 m from the injector outlet [12,13]) and dispersion (velocity and cone angle in the initial region of the spray [13]). As the major contribution, an innovative methodology is presented to measure and reconstruct drop-size distribution: it is based on weighting drop-size over volume-flux distribution, that is determined employing a mechanical patternator. This approach stands as a fully-experimental alternative to the analytic method proposed by Zhu and Chigier [35], which consists of converting linear *Malvern Spraytec* data into point measurements. A distribution function is then introduced to predict the drop-size trend in respect to the spray volume fraction. As an additional remark on the here proposed method, patternation measurements are mentioned by Lefebvre [13] as a major task in spray characterization, providing some quantitative evaluation of the flow spatial distribution at prescribed distances from the nozzle. A classic correlation has also been validated to predict the characteristic SMD of the spray through a physical discussion that follows a model proposed by Lefebvre [13]; like many others, that relation was developed for different applications (e.g.: internal combustion engines) and fluids (e.g.: gasoline, kerosene).

With regard to dispersion, a series of PIV tests has been carried out to evaluate velocity of the water-mist spray in the region right downstream the injector outlet. As the primary scope of this analysis, initial-velocity magnitude has been determined together with its gap in respect to a reference value yielded by an non-viscous

physical model. The extrapolated velocity fields also allow to infer some observations on the spray dynamics, with relation to different spatial shares of the flow. As an additional outcome, an evaluation of the spray-cone angle has been stressed out from velocity profiles, thus strengthening the overall quantification of spray dispersion [13].

As a concluding remark, the main contribution of the present work consists of providing some guidance on the experimental characterization of water-mist sprays, given the few references on this flow typology currently available in the open literature. Both the quantitative results and the proposed relations may be of interest for spray researches, but they are to be ultimately referred to the employed atomizer. As highlighted by Lefebvre [13], the nozzle characteristics (shape, dimensions, etc.) have a strong impact on the investigated phenomena.

2. Experimental facility

An experimental facility has been built to carry out tests on the water-mist spray: a sketch of the whole apparatus is presented in Fig. 1. The nozzle (Fig. 2) has been placed at 2 m height from the floor. This kind of nozzle (CJX 1140 B1SG manufactured by *PNR Italia S.r.l.*) is commonly employed to produce water mist for both fire protection and surface cooling; it consists of seven injectors, six peripheral and one central. Each one is a pressure-swirl atomizer, producing a solid-cone spray; this latter feature is clearly shown by PIV images and maps (Section 4). The detail of the injector front section is also shown in Fig. 2: the water flow moves from the swirl chamber to the exit duct, that has a diameter D_i of 0.5 mm. This latter geometric parameter governs this kind of study, because the flow fulfills the outlet orifice resulting in a solid-cone spray. Finally, a divergent expansion slot follows the exit duct (Fig. 2). Being the present work focused on the spray produced by a water-mist atomizer, the six peripheral injectors have been blocked and tests have been conducted on the central one: this procedure simplifies the experiments, without any lack of physical comprehension on the involved phenomena.

As already mentioned in the introduction, drop-size measurements have been performed employing a *Malvern Spraytec* particle sizer (Fig. 3). This instrument is based on the Fraunhofer-diffraction phenomenon, that occurs when a generic drop impacts a light beam. This latter is issued by a laser emitter (collimated laser diode). The diffraction angle depends on the drop size: the diffraction pattern (Fraunhofer type) consists of a series of concentric rings, that are spaced depending on drop diameter. The light receiver is thus

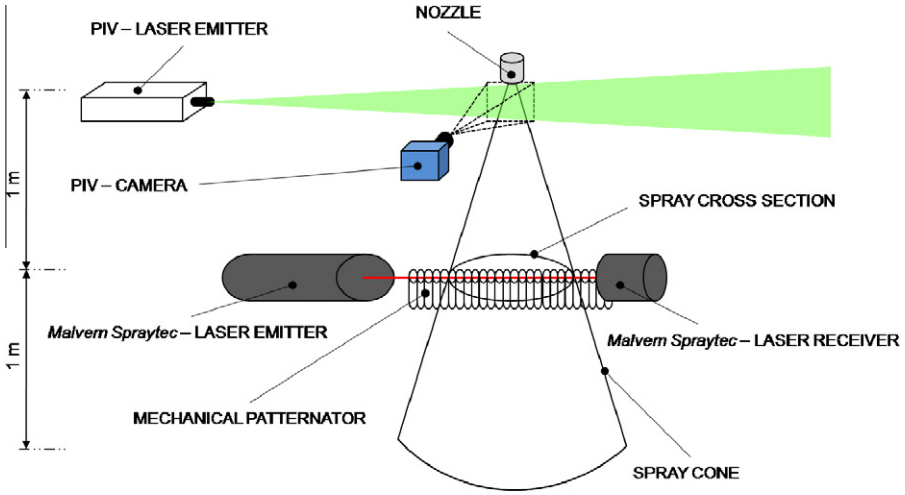

Fig. 1. Sketch of the experimental facility.

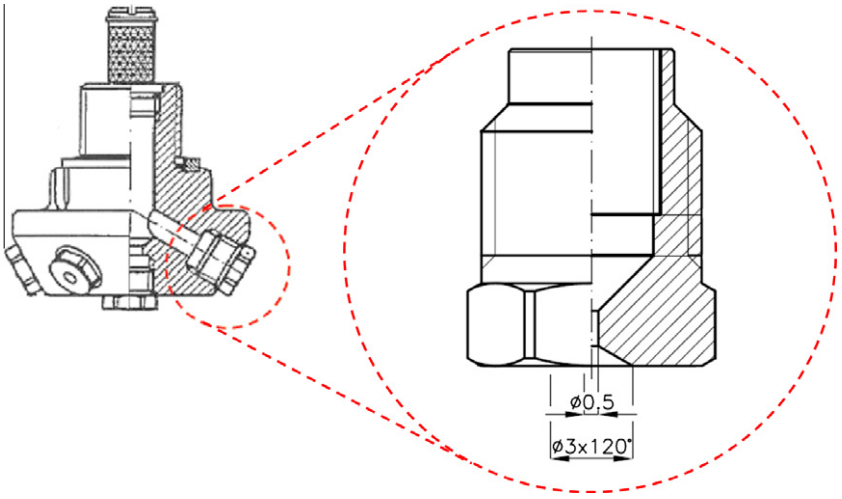

Fig. 2. Technical sketch of the nozzle and detail of the employed injector (dimensions are reported in mm).

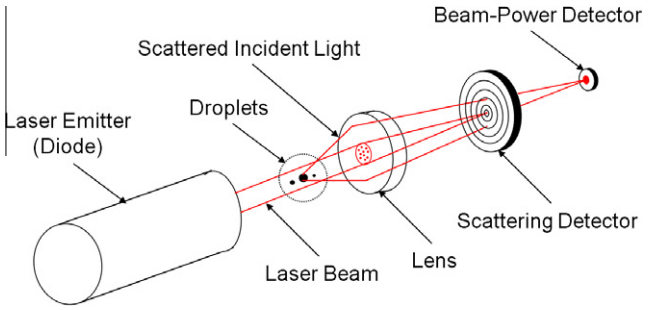

Fig. 3. Sketch of the *Malvern Spraytec* components and functioning (reproduced from [8], adapted from [28]).

constituted by 31 photosensitive rings (being each one related to a definite range of size) and a central circle, which is aimed at detecting the non-affected amount of light. The entire signal is finally focused onto a power detector, that measures attenuation of the incident light, thus estimating the drop concentration. Drop-size distribution is calculated through appropriate correlations referred to intensity distribution (determined by the different rings) and volume fraction (determined by the evaluation of incident light). A detailed description of the related physics and the optical components is provided in Swithenbank et al. [20] and Rinkevichius [22]. The support frame of the *Malvern Spraytec* has been adjusted to set the laser beam onto the spray cross section at 1 m height from the floor: drop-size measurements have been carried out on the plane that lies perpendicular to the central-injector axis at 1 m distance from its outlet. This value has also been proposed in the work by Wang et al. [10], being of interest for design of water-mist systems, as reported in a recognized standard [12].

Velocity measurements have been carried out employing PIV technique. This latter is based on illuminating a flow surface through a laser sheet. Therefore, fluid particles (if reasonably small and sufficiently distinguishable) or tracking particles are clearly visible and their position can be detected and recorded by a camera. Two images of the illuminated flow field allow to reconstruct the motion of a generic particle over the *a priori* determined time distance: velocity is thereby extrapolated. A remarkable survey on physical principles underlying this technique is provided by Adrian [36] and Rinkevichius [22]. The here employed PIV system is constituted by a pulsed-Nd:YAG laser emitter released by *Dantec Dynamics* and a thermo-electrically cooled CCD camera (14 bit, 4 Mpixels) released by *LaVision*. In this facility, the laser emitter and the camera have been set to make the axis of the camera perpendicular to the emitted laser sheet. The laser sheet is focused on the plane containing the injector axis; moreover, the frame has been adjusted to illuminate the initial region of the spray. Energy of 30 mJ matches with each laser pulse; double images have been taken with a time distance of 5 μs one to the other. This optimized interval has been iteratively determined following the guidelines suggested by Keane and Adrian [37]: the average particle motion should stay in the range 4–8 pixels between the two exposures. Velocity maps have been reconstructed averaging a set of 300 double images taken at 4 Hz frequency. The *DaVis 7.2* software by *LaVision* has then been employed to post-process the images: suitable correlations have been applied to extrapolate the velocity field.

Volume- or mass-flux measurements have been carried out through an *ad hoc* built mechanical patternator. This tool is constituted by a set of 55 plastic tubes: each one has an internal diameter of 18 mm and a thickness of 3 mm. The tubes are constrained along a straight row by two plastic beams; the inlet section of each tube lies onto a plane perpendicular to the injector axis. Most notably, the central tube has been placed right under the injector, thus making its axis coincident with the injector one. The frame of the patternator has been adjusted to collect the sprayed water at 1 m height from the floor: therefore, drop-size and flux measurements are consistent as performed on the same spray cross section. This approach has been inspired by Ren et al. [28], even if the spatial extension of that patternator was designed to adapt to traditional-sprinkler sprays, which are characterized by lower mean velocity.

Finally, a data-acquisition system has been added to the apparatus: it has been employed to process both drop-size and velocity measurements. A tank (about 57 l) and an electric pump have been installed to supply the requested amount of water. A pressure gauge has been inserted right upstream the nozzle to control the operative pressure, that is one of the governing parameters in the present work. The experimental tests have been carried out at 60, 70 and 80 bar: these values tend to cover the broad spectrum that stretches from 50 up to 100 bar, which is considered to identify high-pressure water-mist systems from a technical point of view.

3. Drop-size and volume-flux distribution

3.1. Experimental methodology

The sampling volume of the *Malvern Spraytec* is sufficiently wide to cover the entire diameter of the spray. Therefore, the laser beam can be emitted along a diameter of the spray cross section to measure drop-size distribution. However, a potential biasing effect may occur because of the difference between the geometric shape of the laser beam (a cylinder, that may be approximately identified as a line) and the spray section (a circle). Being this instrument capable of evaluating drop size along its sampling volume, the ratio among numbers of particles having the same size might be improperly evaluated with relation to the full section. This potential effect would bias the drop-size vs. Cumulative Volume Fraction (CVF) curve. The definition of Sauter Mean Diameter (SMD), also known as D_{32}, may lead to a direct comprehension of this potential biasing effect:

$$SMD = D_{32} = \frac{\sum_k n_k D_k^3}{\sum_k n_k D_k^2}. \quad (1)$$

In Eq. (1), D_k is the kth drop diameter and n_k is the number of droplets having that diameter. The above described mismatch between sampling and full-spray area could imply an incorrect evaluation of the number of droplets having a given diameter, if compared with other families of droplets characterized by different sizes. In summary, if the ratio among numbers of droplets having the same diameter is the same within the sampling area as over the entire spray section, the SMD is correctly determined; otherwise, the biasing effect occurs resulting in an unreliable evaluation.

A simple procedure has been followed to check the presence of this undesired effect for the considered spray. The *Malvern Spraytec* has been placed along a diameter of the spray cross section at 1 m distance from the injector outlet and drop-size measurements have been carried out varying the length of the sampling volume. Most notably, part of the exposed laser beam has been covered by the insertion of two tubes, one at the end of the emitter, the other at the end of the receiver. Therefore, the effective sampling volume has been varied employing tubes of different length. For each value of operative pressure, the SMD is shown to generally decrease as the sampling length increases (Fig. 4): its variability proves that the described measurement approach yields to biased results. As presented in Fig. 4, the SMD has in fact an initial increase; however, the results related to the shorter length are unrealistic, because most of the droplets do not flow within the

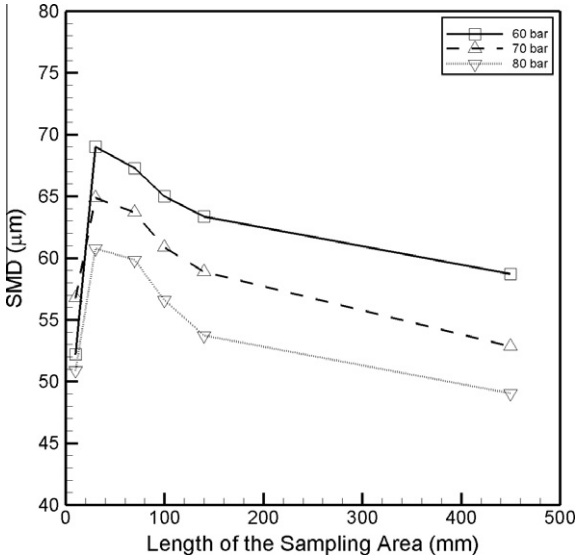

Fig. 4. Trend of SMD as the length of *Malvern Spraytec* sampling area varies.

sampling volume, rather rebounding on the frame of the instrument.

Therefore, an alternative measurement methodology has been developed to gain a proper evaluation of drop size in respect to volume fraction. As a first step of the procedure, drop-size measurements have been taken at a given number of locations along a radius. A representative sketch of this approach is presented in Fig. 5. The length of the sampling volume has been set equal to 30 mm and the *Malvern Spraytec* has been placed perpendicular to the radial coordinate. Location 0 lies at the intersection between the radius and the injector axis; measurements have been conducted every 30 mm ($\Delta r_{Drop\ Size}$) starting from that location along the radial coordinate. The further significant location has been identified at 120 mm from location 0: beyond, particles are too sparse and tiny (the proper mist), thus producing an excessive noise in the output. A set of drop-size curves is thereby obtained, being each one referred to a different location along the radius. It is noteworthy to mention that drop-size measurements at various radial locations were realized by Wang et al. [10] too, even if by PIV technique.

As already mentioned in the introductive section, the flux distribution has been employed as the weighting parameter to reconstruct an overall drop-size distribution for the entire spray. Flux distribution has been evaluated by the mechanical patternator,

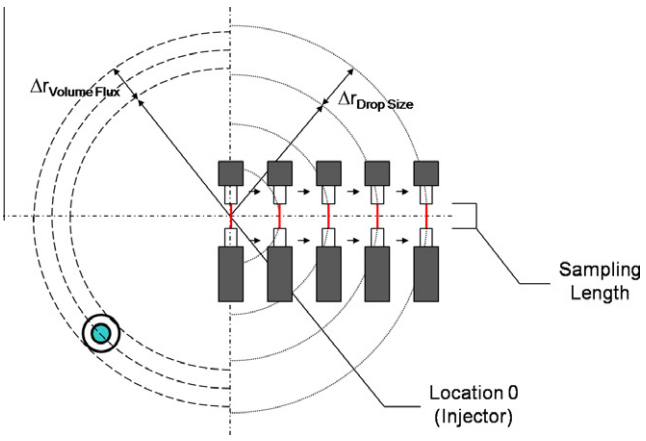

Fig. 5. Sketch of the drop-size and volume-flux measurement procedure.

that has been placed along a diameter of the spray cross section. The measured height of water within each tube yields to both volume and mass flux, being the area of the tube cross section and the operative time *a priori* known. The obtained values have been considered to be valid for the entire circular crown identified by the generic tube (Fig. 5): this circular crown shows a radial extension ($\Delta r_{Volume\ Flux}$), that is equal to the outer diameter of each tube. The radial distance between two consecutive location for drop-size measurement is thus different from the radial validity region of every flux measurement. Therefore, a curve of volume-flux distribution has been finally extrapolated for each operative pressure to obtain the values corresponding to the drop-size-measurement locations. To this end, the volume-flux experimental points have been interpolated through a suitable polynomial (3rd degree) best-approximation curve for every value of operative pressure. The radial distributions of these data together with the resulting curves are presented in Fig. 6.

The final step to reconstruct the overall drop-size distribution as a function of Cumulative Volume Fraction consists of averaging the drop-size measurements over the mass flux, which serves as a sort of weight. The *Malvern Spraytec* can be identified as a particle counter and sizer: it relates a volume fraction (number of particles) to a certain drop size and finally reports a distribution collecting all the shares of the total measured volume. Therefore, the basic idea underlying this procedure is to average each volume fraction through the flux, repeating this operation at every location. First of all, the volumetric flux of all the droplets having the kth size can be expressed as follows:

$$V''_k = \sum_{j=1}^{N} q''_{extr,j} \cdot \frac{1}{\rho} \cdot \frac{\Delta r_{Drop\ Size}}{R_{Drop\ Size}} \cdot VF_{meas,k,j}, \tag{2}$$

where the j index refers to the jth location of drop-size measurements, the subscript *extr* refers to the extrapolation by the best-approximation curve and the subscript *meas* refers to the *Malvern Spraytec* measurements. The distance between two locations of drop-size measurement ($\Delta r_{Drop\ Size}$) has been conveniently made non-dimensional dividing by the maximum radial distance where drop-size measurements are significant ($R_{Drop\ Size}$). The expression for the total volumetric flux is straightforward:

$$V''_{total} = \sum_{k=1}^{M} \sum_{j=1}^{N} q''_{extr,j} \cdot \frac{1}{\rho} \cdot \frac{\Delta r_{Drop\ Size}}{R_{Drop\ Size}} \cdot VF_{meas,k,j}. \tag{3}$$

As the last step, each volume fraction related to the kth drop size is reconstructed as follows:

$$VF_{reconstr,k} = \frac{V''_k}{V''_{total}}. \tag{4}$$

This methodology is physically founded on obtaining the entire volume fraction of the droplets having the same size by multiplying the extrapolated mass flux by the related measured volume fraction at any location and then adding all these values. The procedure has been implemented in a Fortran® code, that allows a rapid processing of both drop-size and mass-flux data at the three values of operative pressure. The ultimate result is a reconstructed drop-size distribution, that refers to the entire spray; any characteristic diameter can be thereby calculated from these data. This methodology stands as a sort of alternative to the analytical approach by Zhu and Chigier [35], that leads to convert *Malvern Spraytec* linear data into point measurements.

A predictive function for the drop-size distribution represents a major task to model the atomization degree of a spray from an experimental set of data. Many studies show that a Rosin–Rammler log-normal distribution is capable of predicting the Cumulative Volume Fraction for sprays and other particle-laden flows with

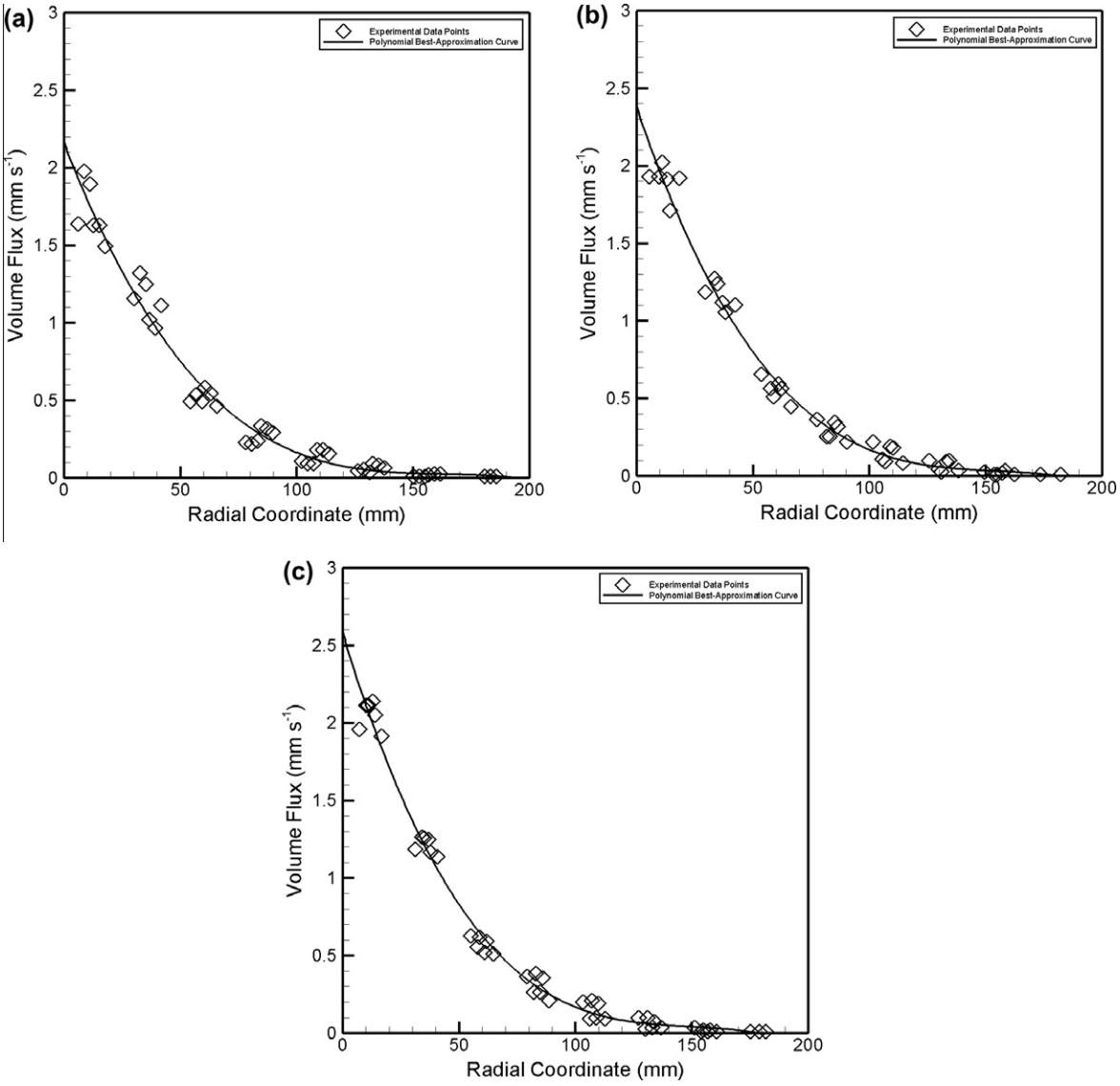

Fig. 6. Radial distribution of volume-flux experimental data and best-approximation curve at (a) 60, (b) 70 and (c) 80 bar of operative pressure.

good agreement with experimental results: among them, it is worthwhile to mention the work by Wu et al. [38] with reference to traditional-sprinkler sprays and the studies by Angeli and Hewitt [39] and Lovick and Angeli [40], which are focused on a very different case (oil–water flows in horizontal pipes). This relation has been employed in the present work because of its successful results in modeling sprinkler sprays, that are physically similar to the water-mist one, in spite of the different operative range of pressure. The Rosin–Rammler log-normal distribution is expressed as follows:

$$CVF = \begin{cases} (2\pi)^{-0.5} \int_0^{D_{CVF}} (\gamma' D)^{-1} e^{-\frac{[\ln(D/D_{v50})]^2}{2\gamma'^2}} dD & (D_{CVF} \leqslant D_{v50}), \\ 1 - e^{-0.693(D_{CVF}/D_{v50})^{\gamma}} & (D_{v50} < D_{CVF}), \end{cases} \quad (5)$$

where γ' is defined as:

$$\gamma' = 2((2\pi)^{0.5}(\ln 2)\gamma)^{-1} = 1.15/\gamma. \quad (6)$$

The curve-fitting coefficient γ in Eq. (5) has to be iteratively determined to obtain the best agreement between the proposed function and the experimental distribution. It is noteworthy to mention that Eq. (6) is an empirical outcome to provide an expression for the γ' parameter.

3.2. Results and discussion

First and foremost, a clarification is ought about the presence of both mass-flux and volume-flux distribution: the former is commonly employed in scientific approaches, because it implicitly takes the fluid density into account. However, an incompressible fluid (water) is here considered; moreover, the unit of volume flux can more easily lead to interpret this parameter as the fluid column collected per time unit: volume flux thus appears to be directly connected to the patternation methodology. The volume-flux distribution is shown in Fig. 7: the presented curves result from an average over the number of tests conducted at each operative pressure. The spray appears to be very symmetric in respect to the injector axis; moreover, variations of operative pressure seem to affect the central peak (maximum value), but not the general shape of the curves. This latter outcome is obviously related with the increase of the released water flow as operative pressure grows.

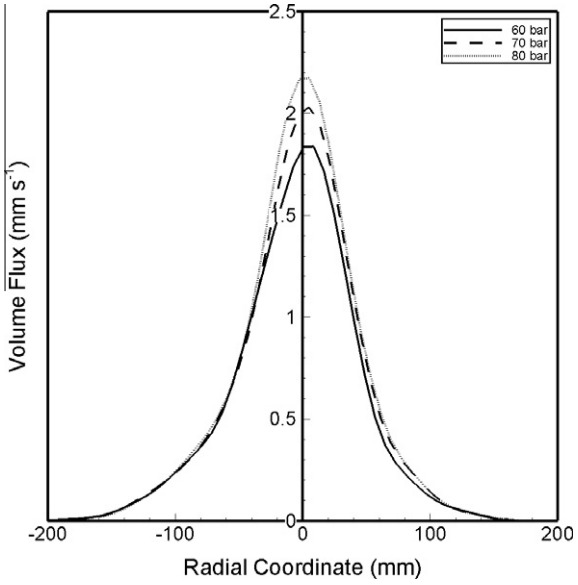

Fig. 7. Average volume-flux distribution.

As shown in Fig. 7, the largest share of the flow is located within the spray cone, while tiny droplets (the proper mist) are spread in the surrounding space. This observation is consistent with the solid-cone spray, even if the distance from the orifice is too wide to completely neglect additional phenomena like coalescence or flow recirculation. With regard to the tinier particles, they tend to evaporate before deeply penetrating the surroundings downstream the outlet (e.g.: the considered spray section at 1 m distance from the orifice). Therefore, the developed patternator may apparently underestimate the flux distribution because of the uncertainty in collecting these droplets; however, their rapid evaporation appears to support the reliability of patternation data, being a share of the flow not anymore part of the spray at the considered location. An integration of the flux measurement over the circular section has been performed taking every measurement as valid for the corresponding circular crown, as already described in Sub-section 3.1. The resulting amount of spray detected through this approach is about 70% of the flow initially released by the injector. The proposed considerations are aimed at providing some insight on flux measurements as a quantitative parameter to understand the spray dynamics and not just a part of a procedure to evaluate drop-size distribution. To this end, a consideration may be drawn

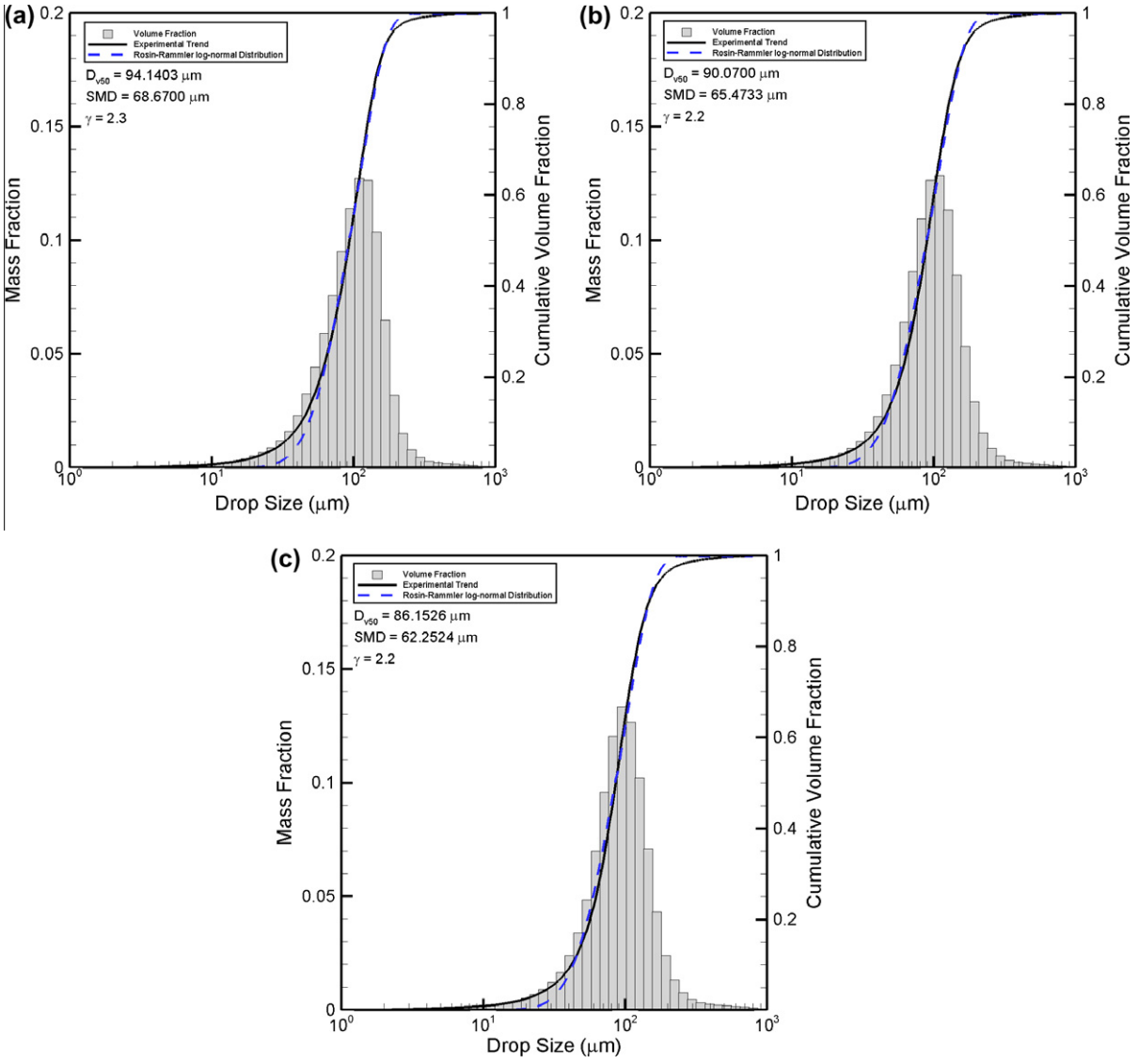

Fig. 8. Drop-size distribution as a function of Cumulative Volume Fraction at (a) 60, (b) 70 and (c) 80 bar of operative pressure.

on the effect the injector geometry may have on flux distribution. As a solid-cone spray, the main geometric parameter is the orifice diameter D_i: its variation may result in different shapes of the curves, implying potential variations in drop-size distribution and thereby in droplet spread over the radial coordinate.

Volume- or mass-flux distribution may also be conveniently employed to validate numerical simulations. Computational models should be capable of tracking the particle motion, at least over a large scale; therefore, their validation may be based on a comparison with experimental data in terms of flow distribution at given locations. Most notably, a code should predict the floating motion of the tinier droplets as well as their rapid evaporation, thus yielding a flux distribution consistent with the measured one. Preliminary validation of computational models are presented by Santangelo et al. [9] with relation to FDS (Fire Dynamics Simulator) and Fluent® codes.

The reconstructed drop-size distribution is presented in Fig. 8 for each value of considered operative pressure. These diagrams result from the already described procedure, that yields to an averaged distribution: therefore, the experimental trend of drop size as a function of Cumulative Volume Fraction appears to be very smooth. As expected, all the distortions due to sparse flow and extremely tiny droplets occurring at the further locations are overtaken by the weighting procedure, thus providing a quantitative representation of the atomization degree for the entire spray. The experimental trend of drop size as a function of the volume fraction yields to a qualitative but immediate evaluation of the droplet amount having sizes lower than a certain value, thus allowing to graphically determine interesting characteristic diameters like the D_{v50} or the D_{v99} [12]. The curve resulting from the Rosin–Rammler log-normal function is also shown in Fig. 8 for each operative pressure. Suitable values of the curve-fitting γ coefficient have been calculated to make the predictive distribution as coincident with the experimental one as possible. A good agreement has been obtained and this outcome is of some importance for two reasons. First of all, if the Rosin–Rammler distribution fits to the experimental data, the developed measurement methodology is implicitly supported, because the drop-size distribution of many different particle flows has been successfully predicted by that function over a variety of studies [38–40]. Moreover, the determined values of γ coefficient are close to values commonly applied to traditional-sprinkler sprays [38], thus emphasizing some quantitative similarity to the water-mist. Therefore, these latter may be approached both as the high-pressure sprays commonly discussed in the propulsion field and as low-pressure sprays of traditional fire-protection applications. The Rosin–Rammler log-normal distribution also serves as a predictive tool for numerical codes to model the atomization degree of the spray: both the function and the obtained values of γ coefficient can be easily implemented to the purpose. Fig. 9 summarizes the obtained results in terms of characteristic diameter (D_{v50} and SMD) and γ coefficient over the considered range of operative pressure. As expected according to atomization physics, the characteristic drop size tends to decrease as operative pressure increases: water-mist systems tend to emphasize this feature more than traditional sprinklers [38], being the imposed static load higher. The quantitative effect of a finer atomization due to pressure increase is about 8.5% in terms of D_{v50} and about 9.3% in terms of SMD between the lower and the upper limit of the considered range of pressure. As a final observation, operative pressure appears not to affect the suitable value of γ coefficient, that is almost constant and equal to 2.2–2.3 over the considered range. With regard to the possible similarity between water-mist and traditional-sprinkler sprays, this outcome seems to support this inference: γ coefficient is generally constant over a wide range of operative pressure for both the cases.

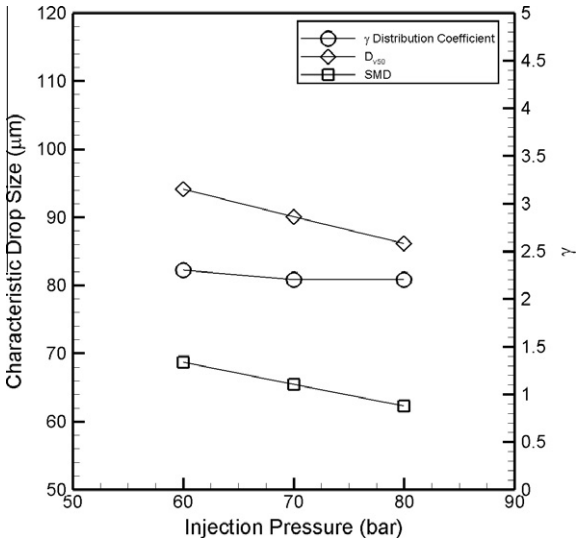

Fig. 9. Trend of D_{v50}, SMD and γ curve-fitting coefficient in respect to operative pressure.

As an additional comment, different orifice diameters may imply different drop-size distributions in terms of size values, even because of the different flow bulk that undergoes the atomization mechanism. However, this variation would impact the characteristic diameters, but the suitability of the Rosin–Rammler function may be unaffected through almost the same curve-fitting values: as already stated, this distribution is applicable to different families of particle flows under the determined governing coefficients.

3.3. Validation of a predictive correlation for the Sauter Mean Diameter

As a final task of the analysis on the atomization degree, a correlation has been validated to predict the SMD. A large number of correlations is available in the open literature about high-pressure sprays; the majority is related to the SMD, being it commonly employed as the characteristic drop size in the propulsion field. Most notably, these relations have usually been developed for fuels (gasoline, kerosene, etc.) rather than other fluids and their applicability to different cases like the present one represents a challenge. With regard to water mist, the classic correlation proposed by Radcliffe [41,13] has been here proposed, showing promising agreement with experimental data:

$$SMD = 7.3 \cdot \sigma^{0.6} \cdot v^{0.2} \cdot \dot{m}^{0.25} \cdot \Delta p^{-0.4}. \tag{7}$$

This relation is one of the earlier and most employed for pressure atomizers in general: for instance, it has recently been applied by Wiksten and Assad [42] to study a water spray for air conditioning and humidifying. The pressure difference Δp refers to the gap occurring between the imposed static load upstream the injector and the ambient pressure. Therefore, this parameter can be assumed to be equal to the value measured by the employed pressure gauge: this latter provides the differential pressure between the fluid and the atmospheric, that is also the one of the surrounding environment. The mass-flow rate can be easily determined from the flow number of the injector:

$$FN = \frac{Q}{\Delta p^{0.5}}. \tag{8}$$

The flow number is usually *a priori* known as a detail released by the nozzle manufacturer; however, it has been measured and proved to be equal to $0.190\,\mathrm{l\,min^{-1}\,bar^{-0.5}}$, with an uncertainty

Table 1
Mass-flow rate and SMD as predicted by the Radcliffe correlation.

	Operative pressure: 60 bar	Operative pressure: 70 bar	Operative pressure: 80 bar
Mass-flow rate $\times 10^2$ (kg s^{-1})	2.46	2.65	2.83
Predicted SMD (μm)	60.06	57.57	55.49

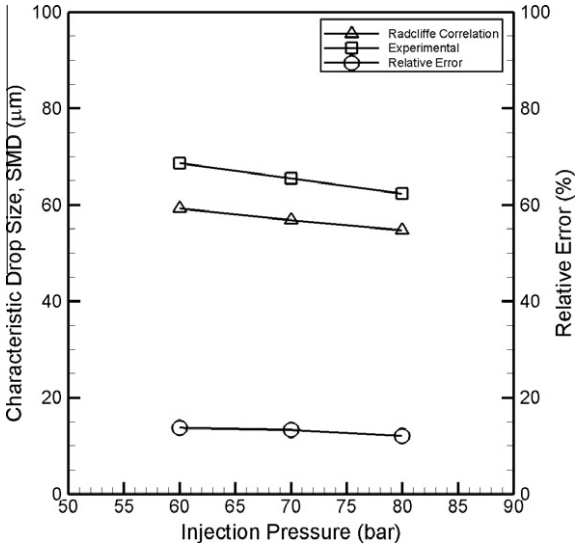

Fig. 10. Comparison between experimental and predicted SMD over the considered range of operative pressure.

range of about 0.002 l min^{-1} bar$^{-0.5}$. This parameter can be assumed as constant over a wide range of operative pressure, typically identified by the operative range of the injector. The values of the discharged mass-flow rate and the predicted SMD are reported in Table 1 for each operative pressure. The trends of experimental and predicted SMD are presented in Fig. 10 as functions of the pressure: they appear to be very consistent one with the other; moreover, the Radcliffe correlation tends to underestimate the SMD with a relative error lower than 15%. This apparent underestimation may be actually due to the drop-size measurements, that have been conducted at 1 m distance from the orifice: secondary atomization and coalescence are two contrasting phenomena and tend to balance with one another; however, this latter may be slightly predominant, even if referred to a high-velocity spray.

The applicability of this empirical correlation is to be assumed as valid for this typology of spray and the employed atomizer: any variation in terms of overall SMD, released mass-flow rate or ultimately injector geometry may yield to different results.

4. Velocity and spray-cone angle

4.1. Experimental methodology

As already mentioned in the introductive section, velocity field and spray-cone angle have been evaluated by PIV technique. The experimental tests have been conducted without addition of seeding particles to the investigated fluid. This choice is commonly applied in multiphase-flow analyses, if one phase consists of a discrete number of particles (bubbles, droplets, pollutant, etc.) [43]. In the present case, water droplets released at high pressure are sufficiently tiny to constitute tracking particles themselves. An example of a PIV image is presented in Fig. 11. The mentioned

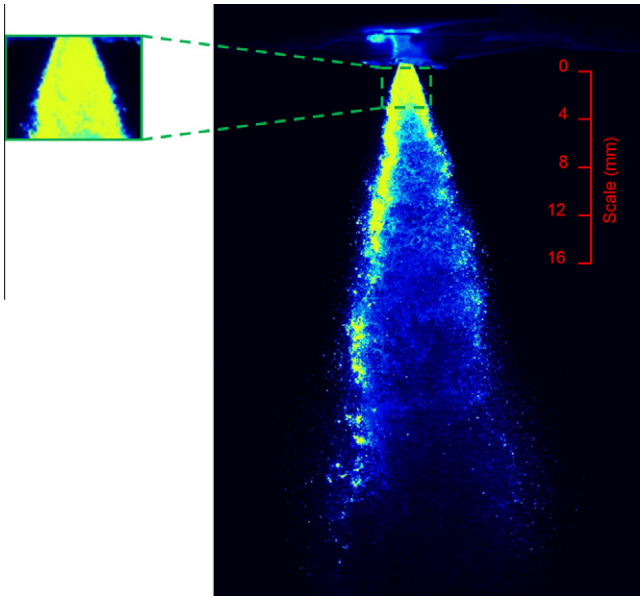

Fig. 11. PIV frame (test at operative pressure of 80 bar) with the dimension scale and a detail of the region right downstream the orifice.

choice is obviously acceptable once the liquid continuum has been fully transformed into a spray jet, that means beyond the breakup location; moreover, the droplet concentration should be sparse enough to allow the software to reconstruct the pattern of each particle. However, as shown in the detail of Fig. 11, particle concentration appears to be very high in the region right downstream the outlet (first 4–5 mm along the axis): this area appears to be almost saturated. Therefore, velocity reconstruction by PIV may not be reliable, because of an incorrect following of the generic-drop motion in the post-processing phase. However, velocity field has been here determined by Laser Speckle Velocimetry (LSV) technique, which was developed as antecedent of PIV: high concentration implies short distance between particles and formation of speckles on the images [44]. The main difference between PIV and LSV is basically seeding concentration [45]: speckle patterns are recorded in the high-density region and a suitable correlation is applied to determine the map of the velocity field. This approach has been also proposed by Paulsen Husted et al. [11].

As mentioned in Section 2 and shown in Fig. 1, the laser sheet has been set to illuminate the plane containing the injector axis. As a first observation, Fig. 11 emphasizes the solid-cone nature of this spray, showing a high concentration of particles within the two-dimensional image of the spray cone. Moreover, this PIV application takes into account the velocity components lying on the illuminated plane. This two-dimensional approach towards a physically three-dimensional vectorial parameter is supported by some previous studies on high-pressure sprays [10,11,33,34]. The radial component is negligible within the injector, because of the small radius of the internal duct [46,47]; therefore, just axial and tangential components may be assumed as significant at the outlet, because of continuity. However, the tangential component tends to rapidly convert into the radial, moving downwards along the axial coordinate, because the angular velocity is proportional to the ratio R_i/R^2, where R_i is the radius of the orifice and R is the radial position of the generic particle once it has been released into the external ambient. As already stated, the radius of the outlet is very small (lower-than-millimetric order of magnitude), thus yielding to a negligible angular velocity even at low axial distance from the orifice (about 3–4 mm). Therefore, velocity can be evaluated with good approximation by a PIV experimental analysis on the already

mentioned plane. Additionally, the axial component is definitely predominant in high-pressure sprays, as quantitatively shown by Presser et al. [31].

The spray-cone angle has been evaluated through a simple geometric procedure, that is based on the velocity profiles at various axial distances from the injector outlet. The interrogation region has been subdivided over four sub-regions, each one having an axial extension of 10 mm (that means 20 D_i), as shown in Fig. 12. The points identified by letters A and B represent the radial locations where velocity turns into 0, as detected in PIV profiles. Therefore, these points are considered to be the extreme boundaries of the spray cone; an evaluation of half cone angle is then straightforward:

$$\theta = \arctan\frac{|x(A_{k+1}) - x(A_k)|}{|y(A_{k+1}) - y(A_k)|}, \quad k = 0, 1, 2, 3. \tag{9}$$

This procedure has been applied to both the sides of the cone, that means both the positive and the negative direction of the x axis (A and B points); a simple average has been calculated for every sub-region: this latter step has been carried out to overtake possible little asymmetries of the spray in respect to the y axis. This evaluation of the spray-cone angle does not result in a proper axial function, but more in a quantitative trend over subsequent zones moving downwards from the outlet. As shown in Fig. 12, the line A_0–B_0 does not perfectly lie onto the outlet section: it stands at a distance of less than 0.5 mm, where PIV vectors start to be effectively present.

4.2. Non-viscous model for velocity magnitude

Inviscid-fluid approximation has been introduced to provide a simple model to evaluate the initial velocity magnitude. Inviscid-flow analyses of sprays produced by pressure atomizers have been proposed in a remarkable number of studies; among them, it is noteworthy to mention the physical discussion by Lefebvre [13], also critically reviewed by Chinn [46,47]. The static load imposed to the flow is very high due to the high supply pressure, thus leading to neglect the friction losses occurring as the spray interacts with the surrounding fluid, which is characterized by low pressure (atmospheric). A comparison with experimental data is presented in Sub-section 4.3 to highlight the extent of this approximation, thus providing a quantitative evaluation of the gap between the model and the experimental results.

A simple Bernoulli equation is employed to the purpose and applied to the inlet and to the outlet sections of the injector:

$$P = p_1 - p_{atm} + \frac{1}{2}\rho V_1^2 = p_2 - p_{atm} + \frac{1}{2}\rho V_2^2. \tag{10}$$

As commonly accepted for the present case [13,46,47], the elevation head is considered as negligible. Holding the assumption of inviscid fluid, total pressure remains constant along the injector: it can be measured by a Pitot tube at any location of the path; however, the experimental facility has been provided with a pressure gauge at the inlet of the nozzle, as described in Section 2. Under the additional simplifying hypothesis of negligible dynamic load at the nozzle inlet, the value measured by the pressure gauge is assumed to be representative of total pressure. Therefore, an expression for velocity at the outlet is yielded by the following equation:

$$V_2 = \left(\frac{2p_{PG}}{\rho}\right)^{0.5}. \tag{11}$$

The calculated values have been reported in Table 2 and assumed as a reference for the experimental values: the applicability of a Bernoulli model to the real spray is thereby verified.

4.3. Results and discussion

The first result of the PIV experimental tests consists of a data set related to velocity vectors within the PIV interrogation region. Velocity components have been determined following the motion of the detected particles (droplets); then, the velocity field (magnitude and direction) has been resolved through the application of suitable correlations over the entire sampling space. These outcomes are shown in Fig. 13 as an example of a PIV contour maps, where some scattered velocity vectors have been added to clearly show the spray motion. Most notably, the map referred to 80 bar operative pressure is presented in Fig. 13 as the most interesting value from the industrial point of view; however, the same quali-

Table 2
Reference velocity from the non-viscous Bernoulli model.

	Operative pressure: 60 bar	Operative pressure: 70 bar	Operative pressure: 80 bar
Velocity magnitude, V_{ref} (m s^{-1})	109.55	118.32	126.49

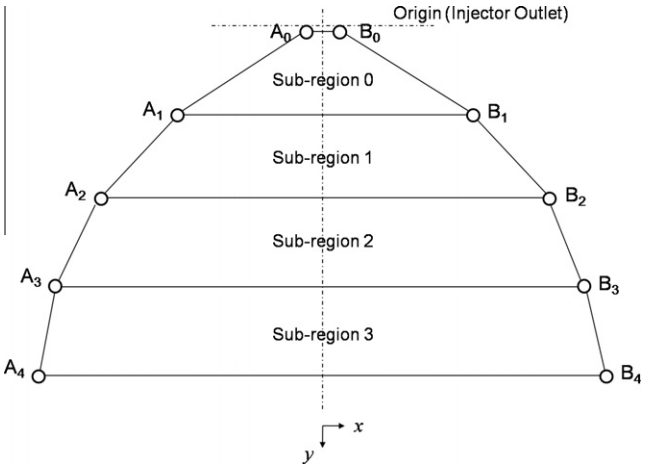

Fig. 12. Sketch of the employed methodology to evaluate the spray-cone angle from PIV velocity profiles.

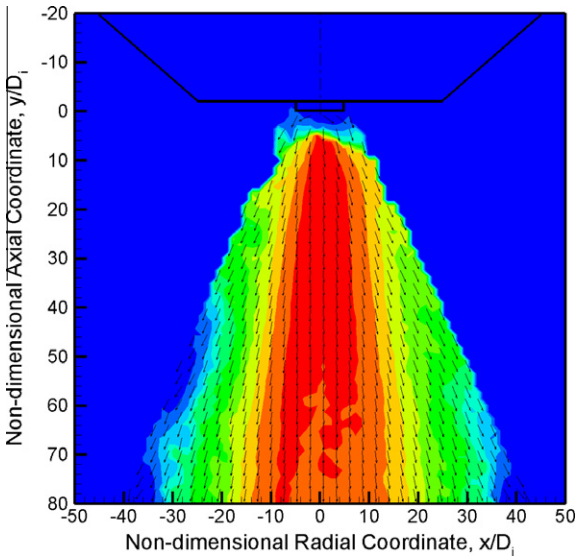

Fig. 13. Vector and contour map of velocity at 80 bar; a simplified sketch of the external geometry of the nozzle is shown as a reference for dimensions.

tative trend was extrapolated at 60 and 70 bar. As a first observation, the central stream around the vertical axis appears to be characterized by the higher velocity magnitude: the motion of this flow is almost completely governed by the imposed momentum, which is ultimately related to the high static load provided by the supply pressure. The droplets located within this zone move straight downwards and deeply penetrate the surroundings; with regard to a fire scenario, these particles tend to generate the flow-flame interaction. On the other hand, the tinier droplets tend to spread radially outwards at low velocity magnitude: they are located in the peripheral sides of the cone (Fig. 13). This share of the flow basically floats within the surrounding fluid (air) and its motion is either buoyancy-driven or alternatively governed by the air streams, which are generated by the entrainment processes and tend to drag the proper mist. With reference to a fire scenario, these droplets tend to rapidly evaporate realizing a cooling effect on the surrounding space, without any interaction with fire. These considerations are consistent with the solid-cone nature of the spray: the flow presents a central stream with the larger droplets, whereas the tinier move at the periphery [13].

The velocity trend moving downwards along the injector axis is summarized in Fig. 14 as radial profiles at different distances from the injector outlet. Velocity magnitude has been made non-dimensional through a ratio by the reference velocity yielded by Eq. (11). First and foremost, operative pressure appears to have a minimal effect on non-dimensional velocity profiles: the presented curves referred to the same distance from the outlet are qualitatively and quantitatively very similar. Moreover, the central zone of each profile is characterized by the higher magnitude, that is in the range 75–80% of reference velocity. Most notably, this peak does not show a remarkable decay while moving axially downwards: this outcome seems to imply a macroscopic conservation of momentum. Therefore, the friction losses due to interaction with the surrounding air do not appear to have a strong effect on velocity magnitude. This latter inference tends to support the proposed inviscid model with relation to the initial region of the spray, which constitutes the PIV sampling area. These outcomes and considerations are emphasized by Fig. 15, that shows initial non-dimensional velocity magnitude. In fact, these maximum values correspond to a distance of about 2.5–3 mm from the injector

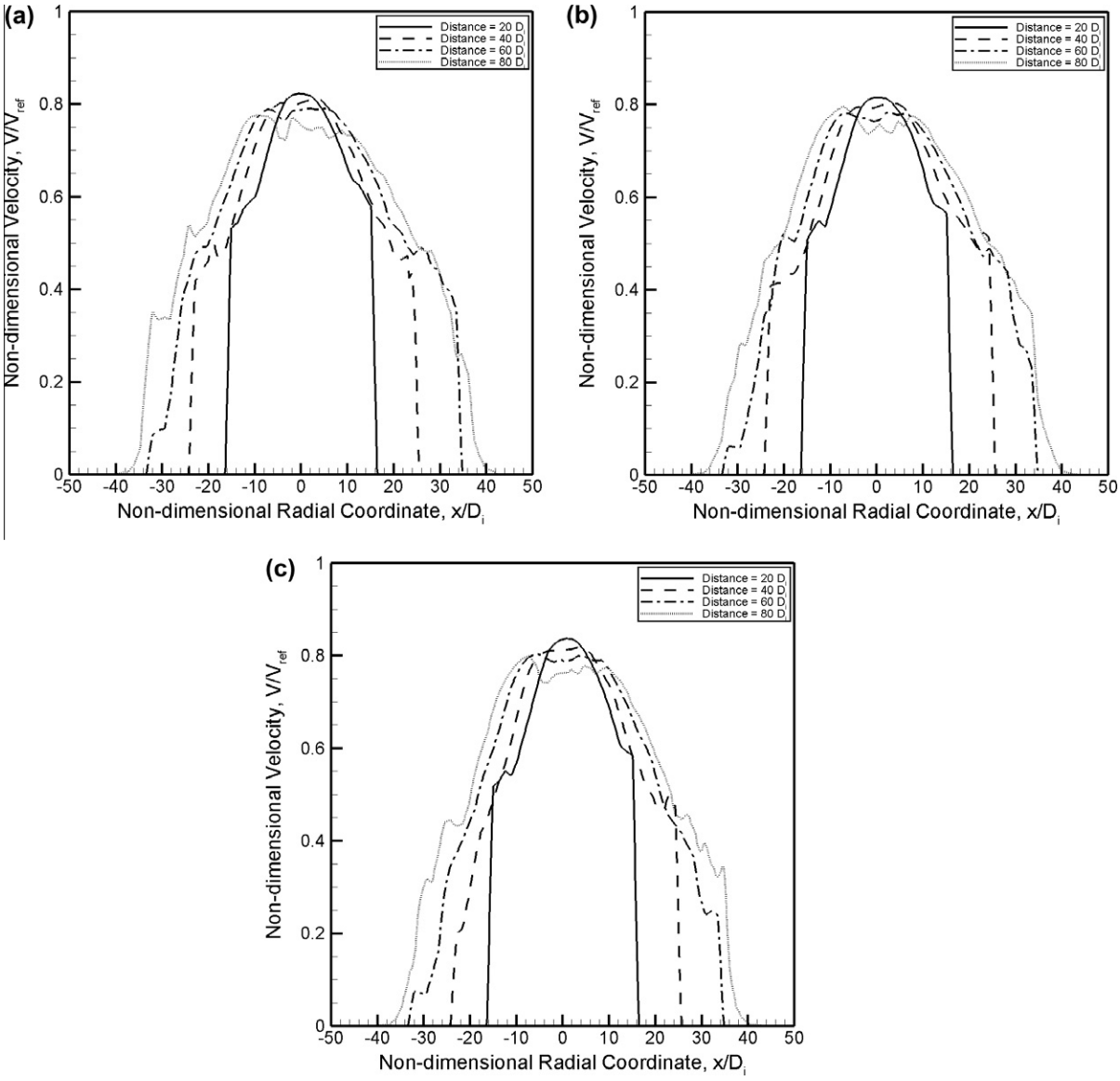

Fig. 14. Radial profiles of non-dimensional velocity at four distances (20 D_i, 40 D_i, 60 D_i and 80 D_i) from the injector outlet for operative pressure of (a) 60, (b) 70 and (c) 80 bar.

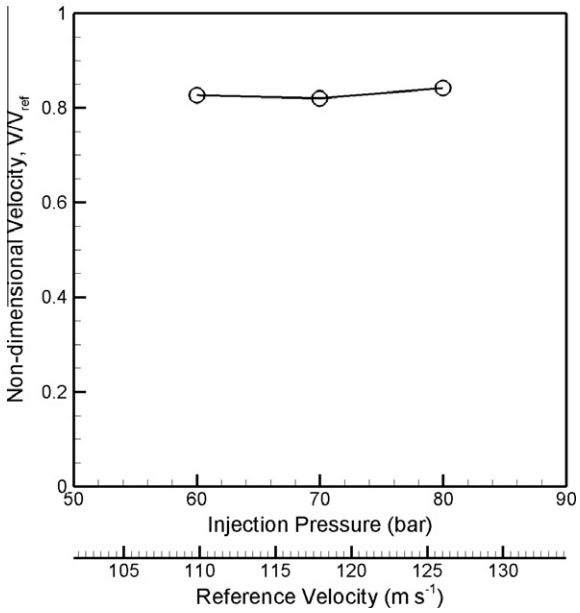

Fig. 15. Initial non-dimensional velocity.

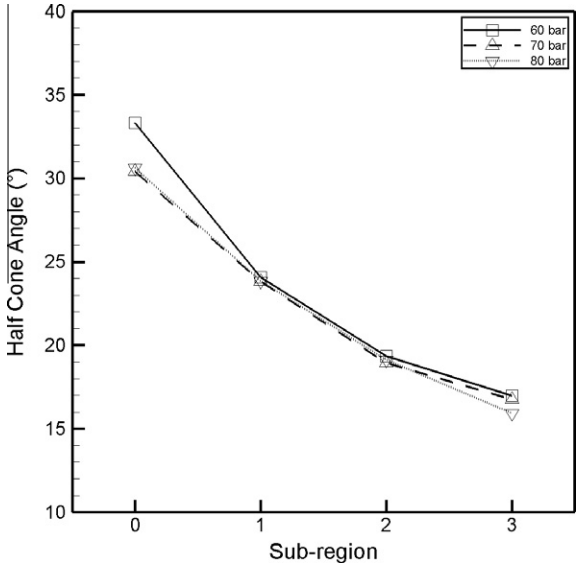

Fig. 16. Trend of the half cone angle over the sub-regions constituting the PIV sampling area.

outlet: as mentioned in Sub-section 4.1, velocity is not reasonably reconstructed within the region right downstream the orifice because droplet concentration is even too high to allow a LSV analysis; moreover, a sort of continuum jet flows upstream the breakup location, thus making PIV technique not applicable to that. The breakup length is expected to be about 2 mm, as evaluated by Wang et al. [10]. Initial non-dimensional velocity appears to be almost constant as operative pressure varies and slightly above 80%: this latter evaluation quantifies the predictive capability of the inviscid model, that may be employed for the initial spray velocity in numerical simulations with an estimated relative error lower than 20%. As a final remark on the velocity analysis, the presented profiles appear to be qualitatively similar to the ones shown by Paulsen Husted et al. [11] for a full-cone nozzle, even though their

Table 3
Evaluated half cone angle over the PIV sampling region.

Sub-region	Operative pressure: 60 bar	Operative pressure: 70 bar	Operative pressure: 80 bar
	Half spray-cone angle (°)		
0	33.31	30.39	30.62
1	24.07	23.82	23.83
2	19.35	18.93	19.14
3	16.98	16.75	15.94

study is focused on a wider sampling area, that starts 25 mm below the outlet. The here investigated injector presents quantitatively higher velocity magnitude than the one in [11] and this difference may be connected to a different orifice diameter (the smaller, the higher velocity is released) or to a different internal shape of the atomizer. For instance, the inclined ducts yielding to the swirl chamber upstream the final duct may have an impact on the velocity field.

The evaluation of the spray-cone angle results from the geometric procedure on the velocity profiles (Fig. 14) and the related outcomes are presented in Fig. 16. Most notably, half cone angle is shown in the diagram to follow classical studies in the field [13,46,47]. The values at the different sub-regions (Fig. 12) are reported in Table 3. As shown by the presented trend, operative pressure does not appear to have a strong effect on the cone angle within the considered range: the same behavior is highlighted for every pressure value, even though the initial angle at 60 bar is slightly higher than the corresponding at 70 and 80 bar. The cone angle tends to decrease as the axial distance from the orifice increases; this trend was expected and is consistent with the classical theory on sprays produced by pressure atomizers [13]: cone angle tends to decrease along the axial coordinate because of the interaction between the sprayed particles and the surrounding fluid. This latter serves as a sort of physical constraint and this effect becomes stronger the further droplets are from the outlet. Quantitatively, the half cone angle is slightly higher than 30° in the initial sub-region, then decreases up to about 16–17° in the further sub-region. It is worthwhile to note that the initial cone angles appear to be lower (about 50%) than the results obtained by Wang et al. [10] in their study on water-mist at low operative pressure (i.e.: 2–8 bar). As already remarked about velocity, the imposed motion has an impact on the spray cone, thus making the internal geometry of the injector a potential governing element. Most notably, the outlet diameter appears to be the most important parameter for solid-cone sprays; in addition, the inclination angle of the ducts yielding to the internal swirl chamber may affect the discharge in terms of initial direction of velocity vectors.

5. Experimental uncertainties and error analysis

As a first clarification, hypothesis of radial and axial symmetry of the spray has been applied to the entire experimental campaign. This assumption is typical in spray analyses, because of the conical shape. The reported volume-flux distribution (Fig. 7) seems to support this simplifying approximation, being the curves very symmetrical to the spray axis. However, these curves result from an average over a large number of tests, that have been conducted to reduce the error and increase precision. Little asymmetries occurred over the numerous tests at every value of operative pressure: differences between positive and negative side of the radial coordinate were present in terms of collected amount of water. The maximum recorded gap is 5%, that leads to consider the hypothesis of radial and axial symmetry as reasonable.

Moreover, percentage dispersion has been calculated for flux distribution to quantify repeatability of these measurements: it is

lower than 4% for each value of operative pressure. On the other hand, a detailed analysis on the accuracy of patternation measurements is very challenging: as already discussed in Sub-section 3.2, the collected amount of water identifies about 70% of the released flow. This result is certainly due to evaporation of the tinier droplets before they reach the spray cross section at 1 m distance from the orifice, but it may also be due to incapability of collecting the tinier droplets within the tubes because of recirculation phenomena (systematic error). However, this latter potential effect would be stronger in the very peripheral regions, where the tinier droplets tend to float, thus not affecting the reconstruction procedure of drop-size distribution, that relates to a radial extension of 120 mm.

The *Malvern Spraytec* is a recognized instrument in particle sizing: its accuracy range is claimed to be lower than 1%, with reference to the D_{v50}, for particle size in the range 0.1–2000 μm. As for patternation, a large set of tests has been carried out to keep control over random variability. The percentage dispersion has been evaluated at every measurement location and for each value of operative pressure: it ranges from 3% to 5%.

With regard to PIV experiments, some limit to the systematic error has been pursued by focusing on a proper alignment of the two pulsed laser sheets constituting the double exposure; moreover, the interval between the two consecutive laser emissions has been optimized, as described in Section 2. A large number of tests has been carried out, each one lasting a considerable time (Section 2), to provide the more precise reconstruction of velocity vectors. The random error is quantified as lower than 5% (data dispersion). Following the discussion by Paulsen Husted et al. [11], the total error in evaluating mean velocity can be estimated as 10%.

Some general expressions of the employed operators to stress out mean values, standard deviation and then percentage dispersion are reported in the Appendix.

6. Conclusions

The present work has been focused on determining some mass-transport characteristics of a water-mist spray produced by a solid-cone pressure atomizer at high injection pressure (60–80 bar). Even though this study mainly refers to fire-protection applications, both the developed methodologies and the obtained results may be of interest for the broad area of high-pressure sprays. Most notably, atomization degree and dispersion have been investigated through an analysis of drop-size and flux distribution, velocity field and spray-cone angle, as suggested by Lefebvre [13] to the purpose.

Optical laser-based techniques have been employed to carry out the experimental tests. A suitable methodology has been developed to reconstruct the overall drop-size distribution of the spray: local measurements have been carried out at different radial locations employing a *Malvern Spraytec* particle sizer; then these results have been averaged over the mass-flux distribution. This latter has been measured by an *ad hoc* built mechanical patternator. This procedure has been proposed to overcome some biasing effects that may occur when measuring drop size along a line over the circular section of a spray; therefore, this approach can be applied to any sprayed flow within a large environment. The characteristic drop size (SMD and D_{v50}) finally resulted from the reconstructed drop-size distribution: this set of results is strongly dependent on the employed injector (mainly the orifice diameter), thus consisting of a specific characterization of the present spray. The same observations may be drawn about flux distribution: the reported trends have a similar shape in respect to operative pressure, even if they quantitatively vary. However, hollow-cone sprays may definitely yield to different curves, given the presence of a strong air core within the spray cone.

A Rosin–Rammler log-normal function has been challenged to reproduce the experimental distribution: the curve-fitting parameter has been calculated to provide the best agreement with the experimental curve and is shown to be almost constant over the considered range of pressure. The proposed function may be conveniently employed for solid-cone water-mist sprays, being typically suitable for a typology of particle-laden flows. As an ultimate outcome, the classic Radcliffe correlation [41] has been evaluated in predicting the SMD: good predictive capability has been stressed out, with little underestimation of the experimental data. However, that relation strongly depends on some dimensional parameters; therefore, its suitability should be verified for different nozzles and spray typologies (hollow cone) before assuming it as of general applicability.

PIV technique has been employed to study the velocity field and to additionally evaluate the spray-cone angle. Some operative considerations have been made to perform PIV tests considering the sole axial and radial components: this approach is applied to a large set of high-pressure sprays. As a first result, the velocity field has been reconstructed in the initial region of the spray, axially stretching over 40–50 mm downstream the injector outlet. A central stream characterized by momentum-driven motion is shown for every value of operative pressure, while other particles are observed to float at low velocity in the peripheral region of the cone. This qualitative outcome is consistent with the behavior of solid-cone sprays in general. The radial profiles of velocity magnitude show that this parameter does not significantly decrease moving downwards along the spray axis: friction losses thus appear not to be remarkably effective in the initial region of the spray. This observation is consistent with other studies on solid-cone water-mist sprays [11].

A model based on inviscid-fluid assumption has also been proposed as inspired by Lefebvre [11] and Chinn [46,47]: it yields to a reference value for initial velocity, that results from a Bernoulli approach. The experimental values are greater than 80% of the reference one over the considered range of operative pressure, thus supporting the reliability of inviscid-fluid approximation. However, this result appears to be peculiar of the investigated injector, whereas other studies report lower velocity magnitude [11]. As expected, the orifice diameter and the motion imposed within the injector may affect the discharge velocity.

The cone angle has been evaluated from PIV velocity profiles over a set of sub-regions constituting the interrogation area. This parameter decreases moving axially downwards, as expected from classical studies on pressure-swirl atomizers [13]. Even if the quantitative values are specifically referred to the employed atomizer, being them related *prima facie* to the injector geometry, the trend can be assumed as generally representative, at least for solid-cone sprays.

The experimental results and the predictive relations may be implemented in numerical codes both to simulate the water-mist spray over the considered range of pressure and to validate the computational models, as preliminary works already show [9].

Acknowledgments

The author wishes to thank Prof. P. Tartarini (Università degli Studi di Modena e Reggio Emilia, Italy), Prof. A.W. Marshall, N. Ren and the entire staff of the FETS (Fire Engineering and Thermal Sciences) Laboratory (University of Maryland, USA) for the guidance and helpful suggestions they provided throughout this work. The financial support by the Italian MIUR, Bettati Antincendio S.r.l., Regione Emilia-Romagna and Fondazione Cassa di Risparmio di Modena is also acknowledged.

Appendix A

The mathematical operators of mean value, standard deviation and percentage dispersion are commonly employed to evaluate the measurement uncertainty, with specific reference to precision [48]. The analytical expressions are the following:

$$MV(\xi) = \frac{\sum_{j=1}^{Z} \xi_j}{Z}, \tag{A.1}$$

$$SD(\xi) = \sqrt{\frac{\sum_{j=1}^{Z} (\xi_j - MV(\xi))^2}{Z-1}}, \tag{A.2}$$

$$Disp(\xi) = \frac{2 \cdot SD(\xi) \cdot 100}{MV(\xi)}. \tag{A.3}$$

The uncertainty analysis has been applied to all the tests conducted at the same value of operative pressure. Most notably, the volume flux has been considered as the specific parameter of investigation for each tube of the mechanical patternator; the spray volume fraction resulting from the *Malvern Spraytec* has been analyzed for each drop-size interval at every measurement location; velocity components have been processed at every spatial location of the PIV sampling area.

References

[1] C.C. Ndubizu, R. Ananth, P.A. Tatem, V. Motevalli, On water mist fire suppression mechanisms in a gaseous diffusion flame, Fire Safety J. 31 (1998) 253–276.
[2] K.C. Adiga, R.F. Hatcher Jr., R.S. Sheinson, F.W. Williams, S. Ayers, A computational and experimental study of ultra fine water mist as a total flooding agent, Fire Safety J. 42 (2007) 150–160.
[3] B.T. Fisher, A.R. Awtry, R.S. Sheinson, J.W. Fleming, Flow behavior impact on the suppression effectiveness of sub-10-μm water drops in propane/air co-flow non-premixed flames, Proc. Combust. Inst. 31 (2007) 2731–2739.
[4] A.M. Lentati, H.K. Chelliah, Dynamics of water droplets in a counterflow field and their effect on flame extinction, Combust. Flame 115 (1998) 158–179.
[5] G.O. Thomas, The quenching of laminar methane–air flames by water mists, Combust. Flame 130 (2002) 147–160.
[6] H.K. Chelliah, Flame inhibition/suppression by water mist: droplet size/surface area, flame structure, and flow residence time effects, Proc. Combust. Inst. 31 (2007) 2711–2719.
[7] P.E. Santangelo, N. Ren, P. Tartarini, A.W. Marshall, Spray characterization of high pressure water mist injectors: experimental and theoretical analysis, in: Proceedings of the 22nd European Conference on Liquid Atomization and Spray Systems – ILASS 2008, Como, Italy, 2008, paper ILASS08-10–5.
[8] P.E. Santangelo, Characterization of water-mist sprays: experimental and theoretical analysis of atomization and dispersion, Doctoral thesis, Università degli Studi di Modena e Reggio Emilia, Modena, Italy, 2009.
[9] P.E. Santangelo, P. Tartarini, B. Pulvirenti, P. Valdiserri, Discharge and dispersion in water-mist sprays: experimental and numerical analysis, in: Proceedings of the 11th Triennial International Conference on Liquid Atomization and Spray Systems – ICLASS 2009, Vail, CO, USA, 2009, paper ICLASS09-051.
[10] X.S. Wang, X.P. Wu, G.X. Liao, Y.X. Wei, J. Qin, Characterization of a water mist based on digital particle images, Exp. Fluids 33 (2002) 587–593.
[11] B. Paulsen Husted, P. Petersson, I. Lund, G. Holmstedt, Comparison of PIV and PDA droplet velocity measurement techniques on two high-pressure water mist nozzles, Fire Safety J. 44 (2009) 1030–1045.
[12] NFPA, NFPA 750: Standard on Water Mist Fire Protection Systems, National Fire Protection Association, Quincy, MA, USA, 2010.
[13] A.H. Lefebvre, Atomization and Sprays, Hemisphere, Washington, DC, USA, 1989.
[14] A.J. Yule, I.R. Widger, Swirl atomizers operating at high water pressure, Int. J. Mech. Sci. 38 (1996) 981–999.
[15] P.K. Senecal, D.P. Schmidt, I. Nouar, C.J. Rutland, R.D. Reitz, M.L. Corradini, Modeling high-speed viscous liquid sheet atomization, Int. J. Multiphase Flow 25 (1999) 1073–1097.
[16] B.J. Azzopardi, Measurement of drop sizes, Int. J. Heat Mass Transfer 22 (1979) 1245–1279.
[17] G.E. Lorenzetto, A.H. Lefebvre, Measurements of drop size on a plain jet airblast atomizer, AIAA J. 15 (1977) 1006–1010.
[18] A.J. Yule, S.M. Aval, A technique for velocity measurement in diesel sprays, Combust. Flame 77 (1989) 385–394.
[19] E. Babinsky, P.E. Sojka, Modeling drop size distributions, Prog. Energy Combust. Sci. 28 (2002) 303–329.
[20] J. Swithenbank, J.M. Beer, D. Abbott, C.G. McCreath, A laser diagnostic technique for the measurement of droplet and particle size distribution, in: Proceedings of the 14th Aerospace Sciences Meeting – American Institute of Aeronautics and Astronautics, Washington, DC, USA, 1976, paper 76–69.
[21] W.D. Bachalo, Experimental methods in multiphase flows, Int. J. Multiphase Flow 20 (1994) 261–295.
[22] B.S. Rinkevichius, Laser diagnostics in fluid mechanics, Begell House, New York City, NY, USA, 1998.
[23] M. Chaker, C.B. Meher-Homji, T. Mee III, Inlet fogging of gas turbine engines – Part II: fog droplet sizing analysis, nozzle types, measurement, and testing, J. Eng. Gas Turbines Power – Trans. ASME 126 (2004) 559–570.
[24] Y. Mori, K. Hijikata, T. Yasunaga, Mist cooling of very hot tubules with reference to through-hole cooling of gas turbine blades, Int. J. Heat Mass Transfer 25 (1982) 1271–1278.
[25] T. Wang, X. Li, Mist film cooling simulation at gas turbine operating conditions, Int. J. Heat Mass Transfer 51 (2008) 5305–5317.
[26] Y.A. Buyevich, V.N. Mankevich, Cooling of a superheated surface with a jet mist flow, Int. J. Heat Mass Transfer 39 (1996) 2353–2362.
[27] N. Sozbir, Y.W. Chang, S.C. Yao, Heat transfer of impacting water mist on high temperature metal surfaces, J. Heat Transfer – Trans. ASME 125 (2003) 70–74.
[28] N. Ren, A. Blum, C. Do, A.W. Marshall, Atomization and dispersion measurements in fire sprinkler sprays, Atom. Sprays 19 (2009) 1125–1136.
[29] W.D. Bachalo, Method for measuring the size and velocity of spheres by dual-beam light scatter interferometry, Appl. Optics 19 (1980) 363–370.
[30] D.T. Sheppard, R.M. Lueptow, Characterization of fire sprinkler sprays using particle image velocimetry, Atom. Sprays 15 (2005) 341–362.
[31] C. Presser, G. Papadopoulos, J.F. Widmann, PIV measurements of water mist transport in a homogeneous turbulent flow past an obstacle, Fire Safety J. 41 (2006) 580–604.
[32] G. Rottenkolber, J. Gindele, J. Raposo, K. Dullenkopf, W. Hentschel, S. Wittig, U. Spicher, W. Merzkirch, Spray analysis of a gasoline direct injector by means of two-phase PIV, Exp. Fluids 32 (2002) 710–721.
[33] K.D. Driscoll, V. Sick, C. Gray, Simultaneous air/fuel-phase PIV measurements in a dense fuel spray, Exp. Fluids 35 (2003) 112–115.
[34] T. Boëdec, S. Simoëns, Instantaneous and simultaneous planar velocity fields measurements of two phases for turbulent mixing of high pressure sprays, Exp. Fluids 31 (2001) 506–518.
[35] H.M. Zhu, N. Chigier, Tomographical transformation of Malvern measurements, Int. Commun. Heat Mass Transfer 13 (1986) 483–491.
[36] R.J. Adrian, Particle-imaging techniques for experimental fluid-mechanics, Annu. Rev. Fluid Mech. 23 (1991) 261–304.
[37] R.D. Keane, R.J. Adrian, Optimization of particle image velocimeters. I. Double pulsed systems, Meas. Sci. Technol. 1 (1990) 1202–1215.
[38] D. Wu, D. Guillemin, A.W. Marshall, A modeling basis for predicting the initial sprinkler spray, Fire Safety J. 42 (2007) 283–294.
[39] P. Angeli, G.F. Hewitt, Drop size distributions in horizontal oil–water dispersed flows, Chem. Eng. Sci. 55 (2000) 3133–3143.
[40] J. Lovick, P. Angeli, Droplet size and velocity profiles in liquid–liquid horizontal flows, Chem. Eng. Sci. 59 (2004) 3105–3115.
[41] A. Radcliffe, Fuel Injection, High Speed Aerodynamics and Jet Propulsion, vol. 11, Section D, Princeton University Press, Princeton, NJ, USA, 1960.
[42] R. Wiksten, M.E.H. Assad, Heat and mass transfer characteristics in a spray chamber, Int. J. Refrig. – Rev. Int. Froid 30 (2007) 1207–1214.
[43] M. Raffel, C. Willert, J. Kompenhans, Particle Image Velocimetry, Springer, Heidelberg, Germany, 1998.
[44] M. Qian, J. Liu, M.-S. Yan, Z.-H. Shen, J. Lu, X.-W. Ni, Q. Li, Y.-M. Xuan, Investigation on utilizing laser speckle velocimetry to measure the velocities of nanoparticles in nanofluids, Opt. Express 14 (2006) 7559–7566.
[45] R.J. Adrian, C.S. Yao, Pulsed laser technique application to liquid and gaseous flows and the scattering power of seed materials, Appl. Optics 24 (1985) 44–52.
[46] J.J. Chinn, An appraisal of swirl atomizer inviscid flow analysis, part 1: the principle of maximum flow for a swirl atomizer and its use in the exposition and comparison of early flow analyses, Atom. Sprays 19 (2009) 263–282.
[47] J.J. Chinn, An appraisal of swirl atomizer inviscid flow analysis, part 2: inviscid spray cone angle analysis and comparison of inviscid methods with experimental results for discharge coefficient, air core radius, and spray cone angle, Atom. Sprays 19 (2009) 283–308.
[48] H.W. Coleman, W.G. Steele, Experimentation and Uncertainty Analysis for Engineers, John Wiley & Sons, New York City, NY, USA, 1999.